A Simple Model for Metal Cation-Phosphate Interactions in Nucleic Acids in the Gas Phase: Alkali Metal Cations and Trimethyl Phosphate

Chunhai Ruan, Hai Huang, and M. T. Rodgers
Department of Chemistry, Wayne State University, Detroit, Michigan, USA

Threshold collision-induced dissociation techniques are employed to determine the bond dissociation energies (BDEs) of complexes of alkali metal cations to trimethyl phosphate, TMP. Endothermic loss of the intact TMP ligand is the only dissociation pathway observed for all complexes. Theoretical calculations at the B3LYP/6-31G* level of theory are used to determine the structures, vibrational frequencies, and rotational constants of neutral TMP and the M^+(TMP) complexes. Theoretical BDEs are determined from single point energy calculations at the B3LYP/6-311+G(2d,2p) level using the B3LYP/6-31G* optimized geometries. The agreement between theory and experiment is reasonably good for all complexes except Li^+(TMP). The absolute M^+–(TMP) BDEs are found to decrease monotonically as the size of the alkali metal cation increases. No activated dissociation was observed for alkali metal cation binding to TMP. The binding of alkali metal cations to TMP is compared with that to acetone and methanol. (J Am Soc Mass Spectrom 2008, 19, 305–314) © 2008 American Society for Mass Spectrometry

Phosphate esters are integral parts of many biologically active molecules ranging from nucleic acids, lipids, and ATP to pesticides and nerve agents [1–3]. Serving as link components in nucleic acids, phosphate esters connect thousands of base pairs to form large molecules that contain the genetic information. These phosphate groups are deprotonated under physiological conditions. The resulting negative charges along the phosphate backbone are stabilized and neutralized by the binding of metal cations. Metal cations can and often do exert a significant influence on nucleic acid structure and genetic information transfer [4]. Metal cation binding reduces the repulsion between neighboring nucleotide units, and therefore influences the stabilization and structural dynamics of nucleic acids and lipids in membranes. For example, alkali and alkaline earth metal cations, including the most biologically important of these cations, Na^+ and Mg^{2+}, prefer to bind to a phosphate group rather than to the nucleobases or sugar moieties [5]. Mg^{2+} is found to increase the melting temperature of DNA [6]. Metal cations may also be involved in the functioning of nucleic acids, e.g., metal cations are required for the proper functioning of all ribozymes [7]. Metal cation-nucleic acid interactions are currently of great interest because metal cations and metal cation-ligand complexes bind to DNA and regulate gene expression, act as drugs, or can be used as tools for molecular biology studies [8]. Hendry and Sargeson studied metal cation-promoted phosphate ester hydrolysis and found that the rate of hydrolysis is modulated by the size of the metal cation and the ease of formation of a four-membered chelate ring [9]. Dempcy and Bruice found a pentacoordinate intermediate for the catalysis of alkyl phosphate diesters [10]. Schneider and Kabelac et al. [11] studied the distribution of five metal cations (i.e., Na^+, Mg^{2+}, K^+, Ca^{2+}, and Zn^{2+}) and water around a negatively charged phosphate group from various crystal structures, and found that all of the cations prefer asymmetric monodentate coordination over bidentate coordination. Their ab initio calculations suggest that bidentate binding of these metal cations to an isolated phosphate group is preferred, but that the presence of even a single water molecule alters this preference. Ab initio calculations of hydrated cations, Mg^{2+} and Ca^{2+}, with dimethyl phosphate also found that cations prefer monodentate binding, as a result of the mutual interaction between the cation, phosphate, and water molecules [12].

To better understand how cation binding influences both the structure and stability of phosphate esters, we have undertaken systematic studies aimed at the characterization of the structures, cation binding affinities, and activation propensities of metal cation-phosphate ester complexes. A wide variety of metal cations are included to examine the influence that the size, charge, and valence electronic structure of the metal cation has on the binding and activation propensities. Thus, the metal cations being investigated include main group metal (Li, Na, K, Rb, Cs, Mg, Al) and transition-metal (Sc, Ti, V, Cr, Mn, Fe, Co, Ni, Cu, and Zn) cations in

Address reprint requests to Dr. M. T. Rodgers, Department of Chemistry, Wayne State University, 5101 Cass Ave., 33 Chemistry, Detroit, MI, USA. E-mail: mrodgers@chem.wayne.edu

1044-0305/08/$32.00
doi:10.1016/j.jasms.2007.10.006

Published online October 22, 2007
Received July 24, 2007
Revised October 6, 2007
Accepted October 10, 2007

their +1 and +2 oxidation states as appropriate. A variety of model phosphate esters are also included to examine the influence that the size, number, and nature of the alkyl groups, the presence of acidic hydrogen atoms, and the charge (neutral versus deprotonated) has upon the binding and activation propensities. Thus, the model phosphate esters being investigated include mono-, di-, and trimethyl phosphate, mono-, di-, and triethyl phosphate, and mono- and di-isopropyl phosphate. In particular, both neutral and deprotonated phosphate esters are included in our studies because although nucleic acids are deprotonated under physiological conditions, the electrostatic interactions between metal cations and the deprotonated phosphate groups are mediated by intermolecular and solvation interactions in the condensed phases, and thus the true nature of the binding is probably stronger than to the neutral, but weaker than to the deprotonated phosphate ester. Because there are several favorable metal cation binding sites on nucleic acids, to the nucleic acid bases, phosphate groups, and sugar moieties, the results of these studies coupled with complementary studies of metal cation binding to nucleic acid bases and sugars should allow rational prediction of the preferred metal cation binding sites to nucleic acids and control over the reactivity and dissociation characteristics of metal cation-nucleic acid complexes.

TMP is a simple phosphate ester that has been extensively studied using a variety of methods including vibrational spectroscopy [13–19], NMR [14, 20], microwave spectroscopy [21], and computational methods [14, 17, 18, 21–24]. Multiple conformers of TMP, designated as C1, C3, and Cs based upon their symmetry, have been found in the condensed and gas phases. In the C3 conformer, all three methyl groups are completely staggered with respect to one another. In the C1 conformer, one of the methyl groups is oriented away from the oxo oxygen, while the other two are staggered with respect to each other. In the Cs conformer, one of the methyl groups is also oriented away from the oxo oxygen atom as in the C1 conformer, but instead of being staggered with respect to each other, the two methyl groups are oriented opposite each other. In the condensed phase, the preferred conformation of TMP is strongly dependent upon the local environment. In solutions, the conformational equilibrium of TMP is strongly influenced by the properties of the solvent. In polar solutions, the C1 conformer is the most stable structure because of its larger dipole moment. In nonpolar environments, the C3 conformer is the most stable conformer. In the gas phase, the ultimate nonpolar medium, the C3 conformer corresponds to the global minimum, the C1 conformer is the next most stable conformer, and the Cs conformer is the least stable low-energy conformer.

In this initial study, trimethyl phosphate (TMP, Figure 1) is used as a simple model for the phosphate groups along the backbone of nucleic acids to study the influence of alkali metal cation binding on the structure and reactivity of phosphate esters in the gas phase. The strength of the interaction of TMP with alkali metal cations is characterized using threshold collision-induced dissociation (TCID) techniques and theoretical electronic structure calculations. The kinetic energy dependences of the collision-induced dissociation (CID) of alkali metal cation–TMP complexes, M^+(TMP), with Xe are examined using a guided ion beam tandem mass spectrometer. The cross sections for endothermic loss of the intact TMP ligand are analyzed using methods previously developed to extract absolute M^+–TMP bond dissociation energies (BDEs) [25]. The trends in the binding of alkali metal cations to TMP are examined and allow determination of the influence of the size of the metal cation on the nature and strength of binding. The binding of alkali metal cations to TMP is also compared with that of acetone [26, 30] and methanol [27–32].

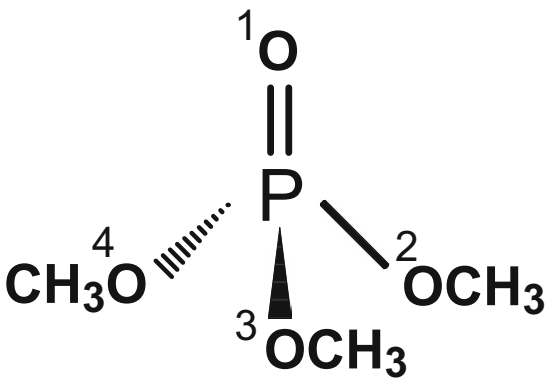

Trimethyl Phosphate (TMP)

Figure 1. Structure of trimethyl phosphosate (TMP).

Experimental

General Procedures

Cross sections for CID of M^+(TMP), where $M^+ = Li^+$, Na^+, K^+, Rb^+, and Cs^+, are measured using a guided ion beam tandem mass spectrometer that has been described in detail previously [33]. Metal cations are generated in a continuous dc discharge by argon cation sputtering of a cathode with a cavity containing the alkali metal (Li, Na, and K) or chloride salt of the alkali metal of interest (RbCl and CsCl). Typical operating conditions of the discharge are 0.5 to 4.0 kV and 5 to 40 mA for alkali metal cation production in a flow of roughly 10% argon in helium. The complexes are generated in a flow tube ion source by condensation of the alkali metal cation and neutral TMP molecule. These complexes are collisionally stabilized and thermalized by in excess of 10^5 collisions with the He and Ar bath gases such that the internal energies of the ions emanating from the source region are believed to be well

described by a Maxwell-Boltzmann distribution at room temperature. The ions are effusively sampled from the source, focused, accelerated, and focused into a magnetic sector momentum analyzer for mass analysis. Mass-selected ions are decelerated to a desired kinetic energy and focused into an octopole ion beam guide. The octopole passes through a static gas cell containing Xe at low-pressure (0.05 to 0.20 mTorr) to ensure that multiple ion-neutral collisions are improbable. The octopole ion guide acts as an efficient trap for ions in the radial direction. Therefore, loss of scattered reactant and product ions in the octopole region is almost entirely eliminated [34–36]. Xe is used here, and in general for all of our CID measurements, because it is heavy and polarizable and therefore leads to more efficient kinetic to internal energy-transfer in the CID process [37–39]. Product and unreacted beam ions drift to the end of the octopole, where they are focused into a quadrupole mass filter for mass analysis, and subsequently detected with a secondary electron scintillation detector and standard pulse counting techniques.

Ion intensities are converted to absolute cross sections using a Beers' law analysis as described previously [40]. Absolute uncertainties in cross section magnitudes are estimated to be ±20%, which are largely the result of errors in the pressure measurement and the length of the interaction region. Relative uncertainties are approximately ±5%.

Ion kinetic energies in the laboratory frame, E_{lab}, are converted to energies in the center of mass frame, E_{CM}, using the formula $E_{CM} = E_{lab}m/(m+M)$, where M and m are the masses of the ionic and neutral reactants, respectively. All energies reported below are in the center-of-mass frame unless otherwise noted. The absolute zero and distribution of the ion kinetic energies are determined using the octopole ion guide as a retarding potential analyzer as previously described [40]. The distribution of ion kinetic energies is nearly Gaussian with FWHM between 0.2 and 0.4 eV (lab) for these experiments. The uncertainty in the absolute energy scale is ±0.05 eV (lab).

Pressure-dependent studies of all CID cross sections examined here were performed because multiple collisions can influence the shape of CID cross sections and the threshold regions are most sensitive to these effects. Data free from pressure effects are obtained by extrapolating to zero reactant pressure, as described previously [41]. Thus, cross sections subjected to thermochemical analysis are the result of single bimolecular encounters.

Theoretical Calculations

To obtain model structures, vibrational frequencies, and energetics for neutral TMP and the M^+(TMP) complexes, simulated annealing and quantum chemical calculations were performed using HyperChem and Gaussian 03 [42]. First, 100 cycles of simulated annealing were performed to find reasonable candidates for the ground state structures. Geometry optimizations and frequency analyses were performed at the B3LYP/6-31G* level for all plausible low-energy neutral TMP and M^+(TMP) candidate structures. For the Rb^+ and Cs^+ complexes, geometry optimizations and frequency analyses were performed using a hybrid basis set in which the effective core potentials (ECPs) and valence basis sets of Hay and Wadt (HW) were used to describe the alkali metal cation [43], while the all-electron 6-31G* basis sets were used for the C, H, P, and O atoms. As suggested by Glendening et al. [44], a single polarization (d) function was added to the Hay-Wadt valence basis set for Rb and Cs, with exponents of 0.24 and 0.19, respectively. The calculated vibrational frequencies were scaled by a factor of 0.9804 [45] and are listed in the Supporting Data, Table 1S (which can be found in the electronic version of this article). Table 2S lists the rotational constants for the ground state conformations. Single point energy calculations at the B3LYP/6-311+G(2d,2p) and B3LYP/6-311+G(2d,2p)-HW levels of theory were performed using the B3LYP/6-31G* and B3LYP/6-31G*-HW optimized geometries. To obtain accurate energetics, zero point energy (ZPE) and basis set superposition error (BSSE) corrections were included in the calculation of the theoretical BDEs [46, 47]. Ground state structures were determined by comparing the absolute energies of the low-energy conformers of neutral TMP and the M^+(TMP) complexes.

The polarizability of the ligand is one of the key factors that influence the strength of metal-ligand binding. A theoretical calculation of the polarizability of TMP based on a dipole electric field was carried out at the PBE0/6-311+G(2d,2p) level of theory. This level of theory was chosen because it has been shown to provide polarizabilities that are in better agreement with experimentally determined polarizabilities than values computed using the B3LYP functional used here for the structures and energetics of these systems [48].

Thermochemical Analysis

The threshold regions of the CID cross sections are modeled using eq 1,

$$\sigma(E) = \sigma_0 \sum_i g_i (E + E_i - E_0)^n / E \quad (1)$$

where σ_0 is an energy independent scaling factor, E is the relative translational energy of the reactants, E_0 is the threshold for reaction of the ground electronic and ro-vibrational state, and n is an adjustable parameter that describes the efficiency of kinetic to internal energy-transfer [49]. The summation is over the ro-vibrational states of the reactant ions, i, where E_i is the excitation energy of each ro-vibrational state and g_i is the population of those states ($\Sigma g_i = 1$).

The Beyer-Swinehart algorithm is used to evaluate the density of ro-vibrational states [50–52], and the relative populations, g_i, are calculated as a Maxwell-Boltzmann distribution at 298 K, the internal temperature of the reactants. The average internal energies at

298 K of neutral TMP and the M^+(TMP) complexes are also given in Table 1S. We have estimated the sensitivity of our analysis to the deviations from the true frequencies by scaling the appropriately prescaled vibrational frequencies (0.9804) by ±10%. The corresponding change in the average vibrational energy is taken to be an estimate of one standard deviation of the uncertainty in vibrational energy (Table 1S) and is included in the uncertainties listed with the E_0 and E_0(PSL) values.

We also consider the possibility that the collisionally activated complex ions do not dissociate on the time scale of the experiment (~100 μs) by including statistical theories for unimolecular dissociation, specifically Rice-Ramsperger-Kassel-Marcus (RRKM) theory, into eq 1 as described in detail elsewhere [25, 53]. The ro-vibrational frequencies appropriate for the energized molecules and the transition states (TSs) leading to dissociation are given in Tables 1S and 2S, where we assume that the TSs are loose and product-like because the interaction between the alkali metal cation and TMP ligand is largely electrostatic. The TS vibrations used are the frequencies corresponding to the products, TMP. The transitional frequencies, those that become rotations of the completely dissociated products, are treated as rotors corresponding to a phase space limit (PSL) as described in detail elsewhere [25].

The model represented by eq 1 is expected to be appropriate for translationally driven reactions [54] and has been shown to reproduce CID cross sections well. The model of eq 1 is convoluted with the kinetic energy distributions of both reactants, and a nonlinear least-squares analysis of the data is performed to give optimized values for the parameters σ_0, E_0, or E_0(PSL) and n. The errors associated with the measurement of E_0 or E_0(PSL) are estimated from the range of threshold values determined for eight zero-pressure-extrapolated datasets, variations associated with uncertainties in the vibrational frequencies (scaling as described above), and the error in the absolute energy scale, 0.05 eV (lab). For analyses that include the RRKM lifetime analysis, the uncertainties in the reported E_0(PSL) values also include the effects of increasing and decreasing the time assumed available for dissociation (~100 μs) by a factor of 2.

Equation 1 explicitly includes the internal energy of the ion, E_i. All energy available is treated statistically because the ro-vibrational energy of the reactants is redistributed throughout the M^+(TMP) complex upon impact with the Xe atom. Because the CID processes examined here are simple noncovalent bond cleavage reactions, the E_0(PSL) values determined by analysis with eq 1 can be equated to 0 K BDEs [37, 55].

Results

Cross Sections for Collision-Induced Dissociation

Experimental cross sections were obtained for the interaction of Xe with five M^+(TMP) complexes, where $M^+ = Li^+$, Na^+, K^+, Rb^+, and Cs^+. Representative data for the Na^+(TMP) complex is shown in Figure 2. The other M^+(TMP) complexes exhibit similar CID behavior and are shown in the Supplementary material, Figure 1S. Over the collision energy range studied, loss of the intact TMP ligand was the only dissociation pathway observed for all five of these systems as summarized in the CID reactions, eq 2.

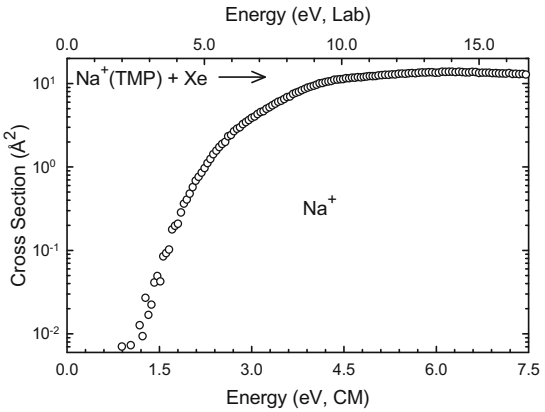

Figure 2. Cross sections for the collision-induced dissociation of Na^+(TMP) with Xe as a function of collision energy in the center-of-mass frame (lower *x*-axis) and laboratory frame (upper *x*-axis). Data for the CID are shown for a Xe pressure of 0.2 mTorr.

$$M^+(TMP) + Xe \rightarrow M^+ + TMP + Xe \quad (2)$$

The apparent threshold for eq 2 is the largest for the Li^+(TMP) complex, and decreases with increasing size of the alkali metal cation. This behavior indicates that the strength of binding in these complexes is inversely correlated with the size of the alkali metal cation as expected for electrostatic binding.

Threshold Analysis

The model of eq 1 was used to analyze the thresholds for eq 2 in five M^+(TMP) systems. The results of these analyses are provided in Table 1. A representative fit to the CID cross section for the Na^+(TMP) complex is shown in Figure 3, while fits to the other M^+(TMP) complexes are shown in the Supplementary material as Figure 2S. In all cases, the experimental cross sections for CID eq 2 are accurately reproduced using a loose PSL TS model [25]. Previous work has shown that this model provides the most accurate assessment of the kinetic shifts for CID processes of electrostatically bound ion-molecule complexes [25, 33]. Good reproduction of the data is obtained over energy ranges exceeding 1.5 eV and cross section magnitudes of at least a factor of 100. Table 1 also lists threshold energies, E_0, obtained without including the RRKM lifetime analysis. Comparison of these values with the E_0(PSL) values shows that the kinetic shifts vary from 0.19 to 1.64 eV across these systems. The number of vibrational

Table 1. Fitting parameters of eq 1, threshold dissociation energies at 0 K, and entropies of activation at 1000 K of M^+(TMP) complexes[a]

Species	σ_0[b]	n[b]	E_0[c] (eV)	E_0(PSL) (eV)	Kinetic shift (eV)	$\Delta S^{\ddagger}$(PSL) (J mol^{-1} K^{-1})
Li^+(TMP)	2.94 (1.1)	1.8 (0.2)	4.55 (0.24)	2.91 (0.15)	1.64	18 (2)
Na^+(TMP)	10.1 (1.0)	1.7 (0.1)	2.36 (0.06)	1.78 (0.06)	0.58	24 (2)
K^+(TMP)	23.9 (1.7)	1.3 (0.1)	1.75 (0.04)	1.40 (0.04)	0.35	19 (2)
Rb^+(TMP)	5.0 (0.8)	1.4 (0.3)	1.57 (0.08)	1.28 (0.06)	0.29	15 (2)
Cs^+(TMP)	2.2 (0.4)	1.7 (0.1)	1.26 (0.06)	1.07 (0.04)	0.19	16 (2)

[a]Uncertainties are listed in parentheses.
[b]Average values for loose PSL transition state.
[c]No RRKM analysis.

frequencies is the same [48] for all of the M^+(TMP) complexes. Because the density of states of the complex at threshold depends on the measured BDE, the kinetic shift is expected to directly correlate with BDE. This is exactly what is observed as summarized in Table 1.

The entropy of activation, $\Delta S^{\ddagger}$, is a measure of the looseness of the TS and also a reflection of the complexity of the system. It is largely determined by the molecular parameters used to model the energized molecule and the TS for dissociation, but also depends on the threshold energy. The $\Delta S^{\ddagger}$(PSL) values at 1000 K are listed in Table 1 and vary from 24 to 15 kJ/mol and are indicative of fairly loose binding.

Theoretical Results

Theoretical structures for neutral TMP and the M^+(TMP) complexes were calculated as described above. Table 2 provides key geometrical parameters of the optimized geometries for the ground state conformers of each of these species. The geometry-optimized structures for several low-energy conformers of neutral TMP and the M^+(TMP) complexes are shown in Figures 4 and 5, respectively.

Several representative low-energy conformers were found for neutral TMP and the M^+(TMP) complexes. In the ground state conformation of neutral TMP, designated as the C3 conformer based upon its symmetry, all three methyl groups are completely staggered to minimize repulsion with each other. Rotation of a single methyl group away from the oxo oxygen atom destabilizes TMP by 4.6 kJ/mol and produces the C1 conformer. Rotation of additional methyl groups leads to even higher energy configurations. When the other two methyl groups of the C1 conformer are oriented opposite each other, designated as the Cs conformer, TMP is further destabilized by 4.2 kJ/mol, and thus lies 8.8 kJ/mol about the ground state C3 conformer. These results are consistent with previous experimental and high-level ab initio calculations [15, 16, 19].

The ground state structure for all of the M^+(TMP) complexes is very similar, and involves interaction of the alkali metal cation with two oxygen atoms, the oxo and one of the alkoxy oxygen atoms. The methyl group of the alkoxy oxygen atom interacting with the alkali metal cation is oriented away from oxo oxygen atom to minimize repulsion with the metal cation, while the other two methyl groups remain staggered to minimize repulsion with each other, such that the TMP ligand takes on a conformation similar to the C1 conformer of neutral TMP in the M^+(TMP) complexes. This presumably occurs so that metal cation can gain additional stabilization by also interacting with the alkoxy oxygen atom. Binding of M^+ to the ground-state C3 Conformer results in monodentate binding to the oxo oxygen atom, and produces a conformation that is only 10.8 kJ/mol less stable than the ground-state conformer for the Na^+(TMP) complex. This suggests that the alkali metal cation-oxo oxygen atom interaction dominates the binding, such that the interaction with the second oxygen atom only enhances the binding by roughly 10%. This interaction is likely to provide a similar amount of relative stabilization energy for all of the M^+(TMP) complexes.

As summarized in Table 2, the metal cation-oxo oxygen (M^+–O1) bond lengths are significantly shorter

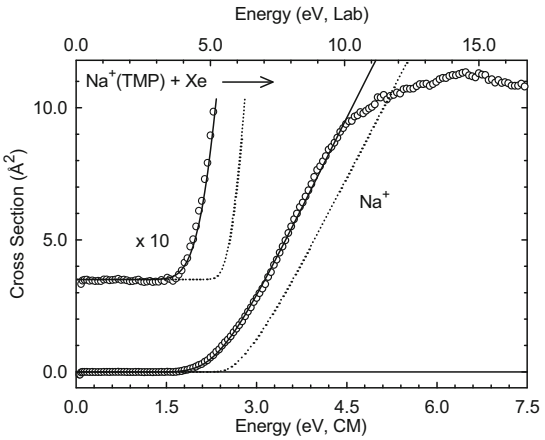

Figure 3. Zero-pressure-extrapolated cross sections for collision-induced dissociation of Na^+(TMP) complex with Xe in the threshold region as a function of kinetic energy in the center-of-mass frame (lower *x*-axis) and laboratory frame (upper *x*-axis). The solid lines show the best fits to the data using eq 1 convoluted over the neutral and ion kinetic and internal energy distributions. The dotted lines show the model cross section in the absence of experimental kinetic energy broadening for reactants with an internal energy corresponding to 0 K.

Table 2. Geometrical parameters of ground state B3LYP/6-31G* optimized structures of TMP and M^+(TMP) complexes

Species	M^+−O1 (Å)	M^+−O2 (Å)	P=O1 (Å)	P−O2 (Å)	C−O2 (Å)	∠MO1P (°)	∠MO2C (°)	∠MO1PO2 (°)
TMP	–	–	1.482	1.606	1.440	–	–	–
Li^+(TMP)	1.745	3.504	1.513	1.582	1.459	145.7	164.7	–22.9
Na^+(TMP)	2.103	3.640	1.503	1.589	1.456	139.2	166.0	–20.4
K^+(TMP)	2.470	4.285	1.498	1.589	1.453	152.8	168.9	–26.1
Rb^+(TMP)	2.708	4.349	1.494	1.593	1.451	148.7	166.0	–21.0
Cs^+(TMP)	2.930	4.488	1.492	1.596	1.450	146.8	164.2	–32.2

than the metal cation-alkoxy oxygen bond lengths (M^+–O2) for all complexes. The M^+−O1 and M^+–O2 bond lengths are found to increase from 1.745 Å to 2.930 Å and 3.504 to 4.488 Å, respectively, as the size of the alkali metal cation increases from Li^+ to Cs^+, while the BDE decreases from 239.0 to 90.8 kJ/mol. Upon binding to TMP, the P=O1 and C–O2 bonds are lengthened by 0.010 to 0.031 and 0.010 to 0.019 Å, respectively, while the P–O2 bonds are shortened by 0.010 to 0.024 Å. The change in bond length is largest for the Li^+(TMP) complex and decreases as the size of the alkali metal cation increases. The metal cations shift away from the other alkoxy oxygen atoms and the ∠MO1PO2 dihedral angle varies from −20.4° to −32.2° as the size of alkali metal cations increases. The size of the alkali metal cation also exerts an influence on the optimized binding geometry of M^+(TMP) complexes. For example, for the Li^+(TMP), Na^+(TMP) and K^+(TMP) complexes, there is one conformation that is very close in stability to the ground state structure, lying only 8.2, 3.8, and 2.6 kJ/mol higher in energy than the corresponding ground state conformers, respectively. The only differences between these low-energy and ground state conformers is that the M^+–O1 bond is lengthened by 0.099, 0.075, and 0.061 Å, while M^+–O2 bond is shortened by 1.417, 1.079, and 1.116 Å, respectively, such that the M^+-oxo oxygen and M^+-alkoxy oxygen atom interactions contribute more equally to the binding. Such low-energy conformers are not found for the larger cations, Rb^+ and Cs^+.

Discussion

Trends in the Binding of Alkali Metal Cations to TMP

The 0 K BDEs of the M^+(TMP) complexes measured here are summarized in Table 3. The variation in the measured BDEs with the size of the alkali metal cation is shown in Figure 6. As can be seen in the figure, the M^+–(TMP) BDEs are found to decrease monotonically as the size of alkali metal cation increases from Li^+ to Cs^+. This can be explained in terms of the electrostatic interactions that control the binding in these complexes. The alkali metal cations have s^0 electron configurations and spherically symmetric electron densities. The alkali metal cation-ligand bond lengths are mainly determined by the size of the cation, such that the larger the cation radius the longer the bond distance, and the weaker the interaction. No activated dissociation of TMP was observed upon alkali metal cation binding, even for the relatively strongly bound Li^+ and Na^+ cations, suggesting that either stronger binding or specific orbital interactions between the metal cation and TMP ligand are required to activate TMP.

Comparison of Theory and Experiment

M^+–(TMP) BDEs at 0 K were calculated at the B3LYP/6-311+G(2d,2p)//B3LYP/6-31G* level of theory including ZPE and BSSE corrections. The theoretical BDEs for the M^+(TMP) complexes are summarized in Table 3

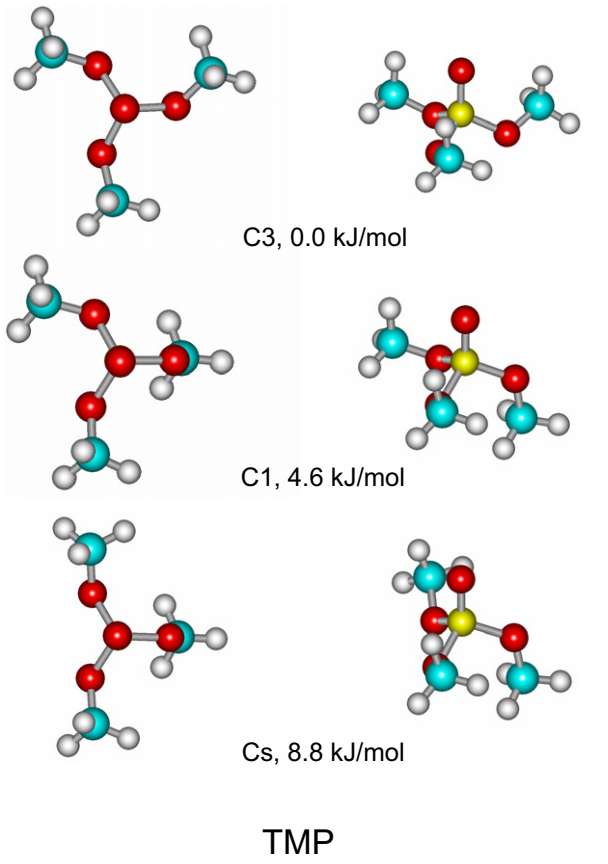

Figure 4. B3LYP/6-31G* optimized geometries of low-energy conformers of TMP. Two views of each structure, their symmetry, and the corresponding B3LYP/6-311+G(2d,2p) relative stabilities are shown.

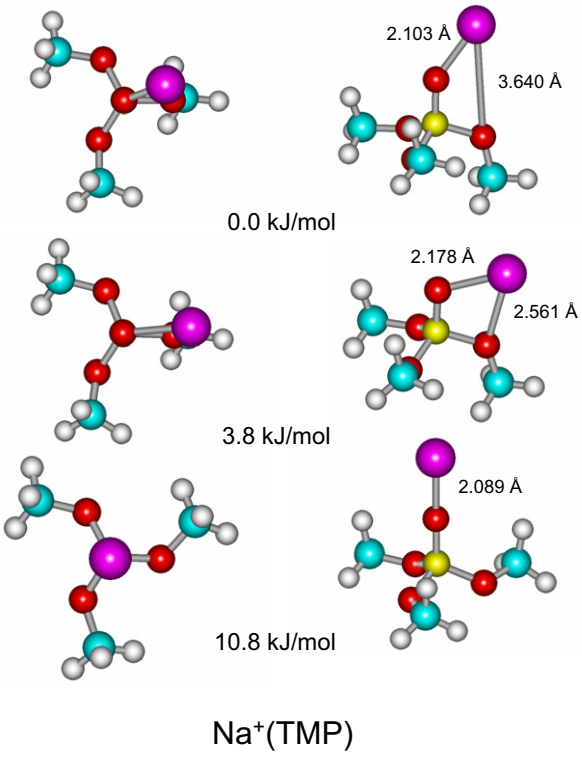

Figure 5. B3LYP/6-31G* optimized geometries of the Na^+(TMP) complexes. Two views of each structure and the corresponding B3LYP/6-311+G(2d,2p) relative stabilities are shown. The Na^+–O1 and Na^+–O2 bond distances are also shown.

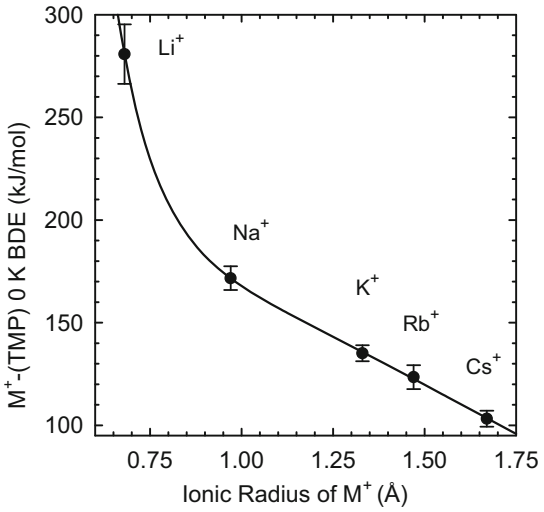

Figure 6. Bond dissociation energies at 0 K (in kJ/mol) of the M^+(TMP) complexes plotted versus the ionic radius of M^+. All values are measured here by TCID and taken from Table 3.

along with the measured values. The agreement between theory and experiment is illustrated in Figure 7. Good agreement between the theoretical and the TCID experimental results is obtained for all of the M^+(TMP) complexes, except Li^+(TMP). The mean absolute deviation (MAD) between theory and experiment for all five complexes is 16.1 ± 15.8 kJ/mol, more than twice the average experimental uncertainty (AEU) in these values, 6.8 ± 4.4 kJ/mol. If Li^+(TMP) is not included, the MAD decreases to 9.6 ± 7.5 kJ/mol. The AEU also decreases to 4.9 ± 1.1 kJ/mol because the experimental error for the Li^+(TMP) complex is larger than other complexes. Clearly the Li^+(TMP) complex is the principal contributor to the MAD. Theory systematically underestimates the BDE of the Li^+(TMP) complex because the basis sets employed in the current study do not allow core correlation, and the higher degree of covalency in the Li^+–(TMP) interactions requires such core correlation to accurately describe the interaction. In an independent study of a number of Li^+(ligand) complexes [56], it was found that complete basis set (CBS) extrapolation of calculations performed at the

Table 3. Enthalpies of alkali metal cation binding to TMP at 0 K in kJ/mol

	Experiment (TCID)	Theory (L=TMP)			Literature	
M^+	(L=TMP)[a]	D_e[b]	D_0[bc]	$D_{0,BSSE}$[bd]	L=Acetone[e]	L=Methanol
Li^+	280.8 (14.5)	246.3	241.2	239.0	203.6	155.3 (8.7)[f]
						159.4[g]
Na^+	171.7 (5.8)	176.6	173.3	170.4	145.7	111.3 (1.0)[h]
					139.7 (1.0)[h]	91.7(5.8)[i]
K^+	135.1 (3.9)	132.5	130.2	128.8	91.9	91.6[j]
						81.4[k]
Rb^+	123.5 (5.8)	107.8	106.0	105.0	82.1	67.4[k]
Cs^+	103.2 (3.9)	94.2	92.2	90.8	74.0	57.9[k]

[a]Present results. Uncertainties are listed in parentheses.
[b]Present results, calculated at the B3LYP/6-311+G(2d,2p)//B3LYP/6-31G* and B3LYP/6-311+G(2d,2p)-HW//B3LYP/6-31G*-HW levels of theory.
[c]Including ZPE corrections with B3LYP/6-31G* frequencies scaled by 0.9804.
[d]Also includes BSSE corrections.
[e]Calculated at the MP2(full)/aug-cc-pVDZ and MP2(full)/(aug-cc-pVDZ,Stuttgart) level of theory, reference [26].
[f]TCID, reference [27].
[g]Ion molecule association reaction, reference [29].
[h]High pressure mass spectrometry, reference [30].
[i]TCID, reference [28].
[j]Ion-molecule association reaction, reference [31].
[k]Calculated at the B3LYP/6-31+G(d) and B3LYP/(6-31+G(d),HW), reference [32].

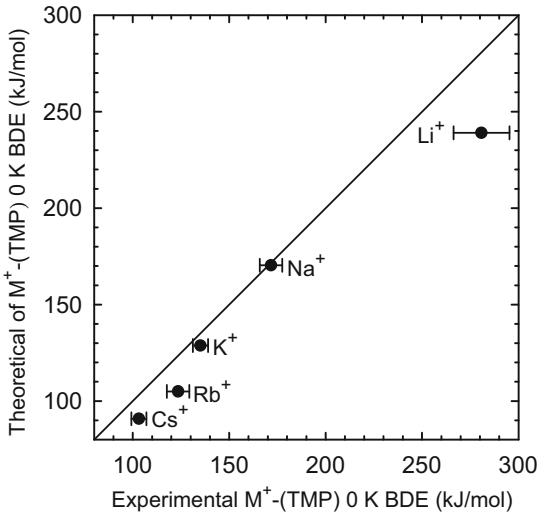

Figure 7. Theoretical versus experimental M^+–(TMP) 0 K bond dissociation energies (in kJ/mol), where $M^+ = Li^+$, Na^+, K^+, Rb^+, and Cs^+. All values are taken from Table 3.

MP2(full)/aug-cc-PVnZ//MP2(full)/cc-PVDZ levels of theory where n = D, T, and Q with additional core correlation functions on Li^+ are necessary to provide accurate BDEs for Li^+(ligand) complexes. However, the G3 level of theory was also found to do a reasonable job even though Li^+ core correlation is not included in the protocol. Unfortunately, calculations at these levels of theory are extremely resource- and time-intensive even for much smaller systems than the M^+(TMP) complexes examined here. Therefore, these advanced calculations were not pursued for the Li^+(TMP) complex in the present study. The experimental results for the Rb^+ and Cs^+ complexes also exhibit somewhat less satisfactory agreement with theory, but much better than that for the Li^+ complex, and is likely the result of the effective core potentials used to describe these two cations. Similar behavior for Rb^+ and Cs^+ complexes has been observed in our previous studies of alkali metal cation binding to other ligands where the BDEs computed using ECPs are found to underestimate the strength of binding [57, 58].

Conversion from 0 to 298 K

The 0 K BDEs determined here are converted to 298 K bond enthalpies and free energies to allow comparison to literature values and commonly employed experimental conditions. The conversions are calculated using standard formulas (assuming harmonic oscillator and rigid rotor models) and the vibrational and rotational constants determined for the B3LYP/6-31G* optimized geometries, listed in Tables 1S and 2S. Table 4S lists the 0 and 298 K enthalpy, free-energy, and enthalpic and entropic corrections for all of the M^+(TMP) complexes experimentally and theoretically determined (from Table 3). Uncertainties are determined by 10% variation in the molecular constants. The trends in the 298 K enthalpies and free energies parallel that found at 0 K.

Comparison of Alkali Metal Cation Binding to Methanol and Acetone

Theoretical calculations suggest that multiple favorable metal cation binding modes to TMP exist for all five alkali metal cations investigated. The ground state conformer involves bidentate binding of M^+ to the oxo and one of the alkoxy oxygen atoms, i.e., the C3 conformer. To dissect the relative contributions of these two interactions to the binding, the M^+(TMP) complexes are compared with the analogous M^+(acetone) [26, 30] and M^+(methanol) complexes [27–32]. The M^+(acetone) complexes are chosen as models for the M^+-oxo oxygen interaction in the M^+(TMP) complexes because the metal cation binds to acetone via a simple monodentate interaction with the carbonyl oxygen atom and there have been no reports of alkali metal cation binding to simple ligands containing a P=O functional group. The M^+(methanol) complexes are chosen as models for the M^+-alkoxy oxygen interaction in the M^+(TMP) complexes because the metal cation binds to methanol via a simple monodentate interaction with the alkoxy oxygen atom. The binding of alkali metal cations to acetone is stronger than to methanol (Table 3), suggesting that interaction with the oxo oxygen atom of TMP should be stronger than with the alkoxy oxygen atom. In addition, the relative M^+–O bond lengths in the ground state conformers of the M^+(TMP) complexes, see Table 2, also suggest that the interaction with the oxo oxygen atom is stronger than with the alkoxy oxygen atom. Finally, the low-energy excited conformers of the M^+(TMP) complexes that involve binding only to the oxo oxygen atom (see for example, the Na^+(TMP) conformer that lies 10.8 kJ/mol above the ground state, Figure 5) are nearly as strongly-bound as the ground state conformers and again suggest that the binding is dominated by the M^+ oxo oxygen atom interaction. The binding of alkali metal cations to TMP is stronger than to acetone (by ~20% to 50%) and significantly stronger than to methanol (by ~60% to 80%). The enhanced binding in the M^+(TMP) complexes as compared with the M^+(acetone) and M^+(methanol) complexes is likely the result of additional stabilization derived from the bidentate binding that occurs in the M^+(TMP) complexes as well as the larger size and thus enhanced polarizability of TMP compared with acetone and methanol. Based on the ground state structures of the M^+(TMP), M^+(acetone) and M^+(methanol) complexes, clearly the alkali metal cations are unable to achieve optimal simultaneous binding to both the oxo and alkoxy oxygen atoms of TMP. The $\angle M^+O1P$ bond angles in the ground state conformations of the M^+(TMP) complexes vary between 139.2° and 152.8°, whereas the $\angle M^+OC$ bond angles are essentially linear in the M^+(acetone) complexes. Similarly, the $\angle M^+O2C$ bond angles in the ground state conformations of the M^+(TMP) complexes vary between 164.2° and 168.9°, whereas the $\angle M^+OC$ bond angles are ~30° to 50° smaller in the

M^+(methanol) complexes. Thus, the bidentate interaction with the alkoxy oxygen atom produces a change in the binding geometry and strength of interaction with both the oxo and alkoxy oxygen atoms that weakens these interactions relative to individual monodentate interactions, but must clearly result in overall stronger binding or such binding geometries would not correspond to the ground state conformers. The steric limitations on the binding result in the BDEs of the M^+(TMP) complexes being ~20% to 30% smaller than the sum of the corresponding M^+(acetone) and M^+(methanol) BDEs. The steric limitations are the greatest for the smallest cations, where the largest deviations from the ideal binding geometries exist, and decrease with increasing size of the alkali metal cation.

Comparison of Alkali Metal Cation Binding to Phosphate Esters in the Gas versus Condensed Phases

In the condensed phases, metal cation-phosphate ester interactions are complicated by intermolecular and solvation interactions. In crystal structures the alkali metal cations bind in a asymmetric monodentate fashion to the deprotonated phosphate group indicating that interaction with water molecules is more favorable than a bidentate interaction with the phosphate group as found for the isolated M^+(TMP) complexes examined here. The interaction of the metal cation with additional water molecules in the condensed phase should further weaken the metal cation-phosphate ester interaction as compared to the isolated species in the gas phase [11,12]. This suggests that the alkali metal cation-phosphate ester interactions in solution are intermediate between the gas-phase interactions of alkali metal cations with the corresponding neutral and deprotonated phosphate esters. According to a quantum chemical and molecular dynamics study [59], 80% of Na^+ cations are almost entirely associated with the phosphate group of DNA and are approximately equally distributed between its first and second solvation shells. This indicates that alkali metal cation binding to the phosphate group is stronger than to water, ensuring that alkali metal cations effectively bind and contribute to the structural stabilization of nucleic acids.

Conclusions

The kinetic energy dependence of the CID of M^+(TMP) complexes, where $M^+ = Li^+$, Na^+, K^+, Rb^+, and Cs^+, with Xe are examined in a guided ion beam tandem mass spectrometer. The loss of the intact TMP ligand is the only dissociation pathway observed for all of these complexes. The thresholds for these dissociation processes are interpreted to yield 0 and 298 K M^+–(TMP) BDEs. The molecular parameters needed for the analysis of experimental data as well as structures and theoretical estimates of the BDEs of the M^+(TMP) complexes are obtained from theoretical calculations performed at the B3LYP/6-311+G(2d,2p)//B3LYP/6-31G* and B3LYP/6-311+G(2d,2p)//B3LYP/6-31G*-HW levels of theory. The agreement between theory and experiment is reasonably good for all complexes except the Li^+(TMP) complex, where theory systematically underestimates the BDE. Rb^+ and Cs^+ complexes also exhibit less satisfactory agreement with theory, probably because of the effective core potentials used to describe these metal cations. The M^+–(TMP) BDEs are observed to decrease monotonically as the size of the alkali metal cation increases from Li^+ to Cs^+. This behavior is explained in terms of the electrostatic nature of the binding. No activated dissociation of TMP was observed upon alkali metal cation binding, even for the relatively strongly bound Li^+ and Na^+ cations, suggesting that either stronger binding or specific orbital interactions between the metal cation and TMP ligand are required to activate TMP. The alkali metal cations prefer to bind in a bidentate fashion to the oxo and one of the alkoxy oxygen atoms of TMP, while for methanol and acetone, monodentate binding occurs. As a result, the strength of alkali metal cation binding to TMP is stronger than to acetone or methanol. However, it is weaker than the sum of the individual binding interactions to these ligands as a result of steric limitations.

Acknowledgments

The authors acknowledge support by the National Science Foundation grant CHE-0518262.

References

1. Chen, W. Q.; Poon, K. F.; Lam, M. H. W. The Application of Solid Phase Microextraction in the Analysis of Organophosphorus Pesticides in a Food Plant. *Environ. Sci. Technol.* **1998,** *32,* 3816–3820.
2. Roast, S. D.; Thompson, R. S.; Donkin, P.; Widdows, J.; Jones, M. B. Toxicity of the organophosphate pesticides chlorpyrifos and dimethoate to *Neomysis integer* (Crustacea: Mysidacea). *Water Res.* **1999,** *33,* 319–326.
3. Brown, M. A.; Brix, K. A. Review of Health Consequences from High-, Intermediate-, and Low-Level Exposure to Organophosphorus Nerve Agents. *J. Appl. Toxicol.* **1998,** *18,* 393–408.
4. Eichhorn, G. L.; Butzow, J. J.; Shin, Y. A. Some Effects of Metal Ions on DNA Structure and Genetic Information Transfer. *Proceedings of the International Symposium of Biomolecular Structure Interactions*; J. Biosci. 1985, *8*(Suppl.), 527–535.
5. *Metal-DNA Chemistry*; Tullius, T. D., Ed.; ACS: Washington, D.C., 1989; 402, p 159.
6. Eichhorn, G. L.; Marzilli, L. G. Advances in Inorganic Chemistry, Vol. 3; Metal Ions in Genertic Information Transfer; Elsevier: New York, 1981; p. 16.
7. Ohndorf, U. M.; Rould, M. A.; He, Q.; Pabo, C. O.; Lippard, S. J. Basis for Recognition of Cisplatin-Modified DNA by High-Mobility-Group Proteins. *Nature* **1999,** *399,* 708–712.
8. Spiro, T. G. Nucleic Acid-Metal Ion Interactions; Wiley: New York, 1980; p. 1 and 31.
9. Hendry, P.; Sargeson, A. M. Metal Ion Promoted Phosphate Ester Hydrolysis. Intramolecular Attack of Coordinated Hydroxide Ion. *J. Am. Chem. Soc.* **1989,** *111,* 2521–2527.
10. Dempcy, R. O.; Bruice, T. C. The Negative Charge of Alkyl Phosphate Diesters and the Slow-Gaited Hydrolysis of RNA and DNA. Catalysis of RNA Hydrolysis Through Metal Ion Ligation to the Ester > PO_2^- Moiety. *J. Am. Chem. Soc.* **1994,** *116,* 4511–4512.
11. Schneider, B.; Kabelac, M. Stereochemistry of Binding of Metal Cations and Water to a Phosphate Group. *J. Am. Chem. Soc.* **1998,** *120,* 161–165.
12. Schneider, B.; Kabelac, M. Hobza, P.. Geometry of the Phosphate Group and Its Interactions with Metal Cations in Crystals and ab Initio Calculations. *J. Am. Chem. Soc.* **1996,** *118,* 12207–12217.
13. Streek, R.; Barnes, A. J.; Herrebout, W. A.; van der Veken, B. J. Conformational Behavior of Trimethyl Phosphate Studied by Infrared Spectroscopy. *J. Mol. Struct.* **1996,** *376,* 277–287.

14. Mastrantonio, G.; Della Vedova, C. O. Spectroscopic and Conformational Comparative Study of Trimethyl Chalcogen Phosphates. *J. Mol. Struct.* **2001,** *561,* 161–174.
15. George, L.; Sankaran, K.; Viswanathan, K. S.; Mathews, C. K. Matrix-Isolation Infrared Spectroscopy of Organic Phosphates. *Appl. Spectrosc.* **1994,** *48,* 7–12.
16. Reva, I.; Simao, A.; Fausto, R. Conformational Properties of Trimethyl Phosphate Monomer. *Chem. Phys. Lett.* **2005,** *406,* 126–136.
17. Sablinskas, V.; Horn, A.; Klaeboe, P. Conformational Stability of Trimethyl Phosphate Studied by Vibrational Spectroscopy and ab Initio Calculations. *J. Mol. Struct.* **1995,** *349,* 157–160.
18. Sankaran, K.; Vidya, V.; Viswanathan, K. S.; George, L.; Singh, S. Trimethyl Phosphate–Water Interaction: A Matrix-Isolation Infrared and Ab Initio Study. *J. Phys. Chem. A* **1998,** *102,* 2944–2953.
19. Vidya, V.; Sankaran, K.; Viswanathan, K. S. Matrix Isolation-Supersonic Jet Infrared Spectroscopy: Conformational Cooling in Trimethyl Phosphate. *Chem. Phys. Lett.* **1996,** *258,* 113–117.
20. Khetrapal, C. L.; Govil, G.; Yeh, H. J. C. The Preferred Conformation(s) of Trimethyl Phosphate as Derived from NMR Spectra of Partially Oriented Molecules and Potential Energy Calculations. *J. Mol. Struct.* **1984,** *116,* 303–311.
21. Aroney, M. J.; Chia, L. H. L.; Le Fevre, R. J. W.; Saxby, J. D. Molecular Polarizability. The Dipole Moments, Molar Kerr Constants, and Conformations of Eleven Phosphate and Phosphite Triesters as Solutes in Benzene. *J. Chem. Soc.* **1964,** 2948–2954.
22. Van Wazer, J. R.; Ewig, C. S. Ab Initio Structures of Phosphorus Acids and Esters. II. Methyl Phosphinate, Dimethyl Phosphonate, and Trimethyl Phosphate. *J. Am. Chem. Soc.* **1986,** *108,* 4354–4360.
23. Gorenstein, D. G.; Kar, D.; Luxon, B. A.; Momii, R. K. Conformational Study of Cyclic and Acyclic Phosphate Esters. CNDO/2 Calculations of Angle Strain and Torsional Strain. *J. Am. Chem. Soc.* **1976,** *98,* 1668–1673.
24. George, L.; Viswanathan, K. S.; Singh, S. Ab Initio Study of Trimethyl Phosphate: Conformational Analysis, Dipole Moments, Vibrational Frequencies, and Barriers for Conformer Interconversion. *J. Phys. Chem. A* **1997,** *101,* 2459–2464.
25. Rodgers, M. T.; Ervin, K. M.; Armentrout, P. B. Statistical Modeling of Collision-Induced Dissociation Thresholds. *J. Chem. Phys.* **1997,** *106,* 4499–4508.
26. Song, J. H.; Kim, J.; Seo, J.; Lee, J. Y. Ab Initio Study on the Structures, Energies, and Vibrational Frequencies of Acetone Complexes with Metal Monocations and Dications. *J. Mol. Struct. (Theochem.)* **2004,** *686,* 147–151.
27. Rodgers, M. T.; Armentrout, P. B. Absolute Binding Energies of Lithium Ions to Short Chain Alcohols, $C_nH_{2n+2}O$, n = 1–4, Determined by Threshold Collision-Induced Dissociation. *J. Phys. Chem. A* **1997,** *101,* 2614–2625.
28. Rodgers M. T.; Armentrout, P. B. Absolute Binding Energies of Sodium Ions to Short Chain Alcohols, $C_nH_{2n+2}O$, n = 1–4, Determined by Threshold Collision-Induced Dissociation. *J. Phys. Chem. A* **1999,** *103,* 4955–4963.
29. Keesee, R. G.; Castleman, A. W., Jr. Thermochemical Data on Gas Phase Ion-Molecule Association and Clustering Reactions. *J. Phys. Chem. Ref. Data* **1986,** *15,* 1011–1071.
30. Guo, B. C.; Conklin, B. J.; Castleman, A. W., Jr. Thermochemical Properties of Ion Complexes $Na^+(M)_n$ in the Gas Phase. *J. Am. Chem. Soc.* **1989,** *111,* 6506–6510.
31. Evans, D. H.; Keese, R. G.; Castleman, A. W., Jr. Thermodynamics of Gas-Phase Mixed-Solvent Cluster Ions: Water and Methanol on Potassium (1+) and Chloride and Comparison to Liquid Solutions. *J. Phys. Chem.* **1991,** *95,* 3558–3564.
32. Cabaleiro-Lago, E. M.; Rodriguez-Otero, J. An Ab Initio Study of $M^+(CH_3OH)_n$ Clusters (M = K, Rb, Cs). Competition Between Interior and Surface Structures. *J. Phys. Chem. A* **2002,** *106,* 7195–7203.
33. Rodgers, M. T. Substituent Effects in the Binding of Alkali Metal Ions to Pyridines, Studied by Threshold Collision-Induced Dissociation and ab Initio Theory: The Methylpyridines. *J. Phys. Chem. A* **2001,** *105,* 2374–2383.
34. Teloy, E.; Gerlich, D. Integral Cross Sections for Ion-Molecule Reactions. I. The Guided Beam Technique. *Chem. Phys.* **1974,** *4,* 417–427.
35. Gerlich, D. Thesis (Diplomarbeit), University of Freiburg, Germany, 1971.
36. Gerlich, D. In *State-Selected and State-to-State Ion-Molecule Reaction Dynamics, Part I. Experiment*; Ng, C.-Y., Baer, M., Eds.; Advances in Chemical Physics Series; Wiley: New York, 1992; 82 p 1.
37. Dalleska, N. F.; Honma, K.; Armentrout, P. B. Stepwise Solvation Enthalpies of Protonated Water Clusters: Collision-Induced Dissociation as an Alternative to Equilibrium Studies. *J. Am. Chem. Soc.* **1993,** *115,* 12125–12131.
38. Aristov, N.; Armentrout, P. B. Collision-Induced Dissociation of Vanadium Monoxide Ion. *J. Phys. Chem.* **1986,** *90,* 5135–5140.
39. Hales, D. A.; Armentrout, P. B. Effect of Internal Excitation on the Collision-Induced Dissociation and Reactivity of Co^{2+}. *J. Cluster. Sci.* **1990,** *1,* 127–142.
40. Ervin, K. M.; Armentrout, P. B. Translational Energy Dependence of $Ar^+ + XY \rightarrow ArX^+ + Y$ (XY = H_2, D_2, HD) from Thermal to 30 eV C.M. *J. Chem. Phys.* **1985,** *83,* 166–189.
41. Dalleska, N. F.; Honma, K.; Sunderlin, L. S.; Armentrout, P. B. Solvation of Transition Metal Ions by Water. Sequential Binding Energies of $M^+(H_2O)_x$ (x = 1–4) for M = Ti to Cu Determined by Collision-Induced Dissociation. *J. Am. Chem. Soc.* **1994,** *116,* 3519–3528.
42. Gaussian 03, Revision C.01, Frisch, M. J.; Trucks, G. W.; Schlegel, H. B.; Scuseria, G. E.; Robb, M. A.; Cheeseman, J. R.; Montgomery, J. A.; Vreven, Jr., T.; Kudin, K. N.; Burant, J. C.; Millam, J. M.; Iyengar, S. S.; Tomasi, J.; Barone, V.; Mennucci, B.; Cossi, M.; Scalmani, G.; Rega, N.; Petersson, G. A.; Nakatsuji, H.; Hada, M.; Ehara, M.; Toyota, K.; Fukuda, R.; Hasegawa, J.; Ishida, M.; Nakajima, T.; Honda, Y.; Kitao, O.; Nakai, H.; Klene, M.; Li, X.; Knox, J. E.; Hratchian, H. P.; Cross, J. B.; Adamo, C.; Jaramillo, J.; Gomperts, R.; Stratmann, R. E.; Yazyev, O.; Austin, A. J.; Cammi, R.; Pomelli, C.; Ochterski, J. W.; Ayala, P. Y.; Morokuma, K.; Voth, G. A.; Salvador, P.; Dannenberg, J. J.; Zakrzerski, V. G.; Dapprich, S.; Daniels, A. D.; Strain, M. C.; Farkas, O.; Malick, D. K.; Rabuck, A. D.; Raghavachari, K.; Foresman, J. B.; Ortiz, J. V.; Cui, Q.; Baboul, A. G.; Clifford, S.; Cioslowski, J.; Stefanov, B. B.; Liu, G.; Liashenko, A.; Piskorz, P.; Komaromi, I.; Martin, R. L.; Fox, D. J.; Keith, T.; Al-Laham, M. A.; Peng, C. Y.; Nanayakkara, A.; Challacombe, M.; Gill, P. M. W.; Johnson, B.; Chen, W.; Wong, M. W. Gonzalez, C.; and Pople, J. A. Gaussian, Inc., Wallingford, CT, 2004.
43. Hay, P. J.; Wadt, W. R. Ab Initio Effective Core Potentials for Molecular Calculations. Potentials for K to Au Including the Outermost Core Orbitals. *J. Chem. Phys.* **1985,** *82,* 299–301.
44. Glendening, E. D.; Feller, D.; Thompson, M. A. An ab Initio Investigation of the Structure and Alkali Metal Cation Selectivity of 18-Crown-6. *J. Am. Chem. Soc.* **1994,** *116,* 10657–10669.
45. Foresman, J. B.; Frisch, M. J. Exploring Chemistry with Electronic Structure Methods, 2nd ed.; Gaussian: Pittsburgh, PA, 1996; p 64.
46. Boys, S. F.; Bernardi, F. The Calculations of Small Molecular Interaction by the Difference of Separate Total Energies. Some Procedures with Reduced Error. *Mol. Phys.* **1970,** *19,* 553–566.
47. van Duijneveldt, F. B.; van Duijneveldt-van de Rijdt, J. G. C. M.; van Lenthe, J. H. State of the Art in Counterpoise Theory. *Chem. Rev.* **1994,** *94,* 1873–1885.
48. Smith, S. M.; Markevitch, A. N.; Romanov, D. A.; Li, X.; Levis, R. J.; Schlegel, H. B. Static and Dynamic Polarizabilities of Conjugated Molecules and Their Cations. *J. Phys. Chem. A* **2004,** *108,* 11063–11072.
49. Muntean, F.; Armentrout, P. B. Guided Ion Beam Study of Collision-Induced Dissociation Dynamics: Integral and Differential Cross Sections. *J. Chem. Phys.* **2001,** *115,* 1213–1228.
50. Beyer, T.; Swinehart, D. F. Number of Multiply-Restricted Partitions [A1]. *Commun. ACM* **1973,** *16,* 379.
51. Stein, S. E.; Rabinovitch, B. S. Accurate Evaluation of Internal Energy Level Sums and Densities Including Anharmonic Oscillators and Hindered Rotors. *J. Chem. Phys.* **1973,** *58,* 2438–2455.
52. Stein, S. E.; Rabinovitch, B. S. On the Use of Exact State Counting Methods in RRKM Rate Calculations. *Chem. Phys. Lett.* **1977,** *49,* 183–188.
53. Khan, F. A.; Clemmer, D. E.; Schultz, R. H.; Armentrout, P. B. Sequential Bond Energies of Chromium Carbonyls $(Cr[CO]_x^+$, x = 1–6). *J. Phys. Chem.* **1993,** *97,* 7978–7987.
54. Chesnavich, W. J.; Bowers, M. T. Theory of Translationally Driven Reactions. *J. Phys. Chem.* **1979,** *83,* 900–905.
55. Armentrout, P. B.; Simons, J. Understanding Heterolytic Bond Cleavage. *J. Am. Chem. Soc.* **1992,** *114,* 8627–8633.
56. Rodgers, M. T.; Armentrout, P. B.. A Critical Evaluation of the Experimental and Theoretical Determination of Lithium Cation Affinities. *Int. J. Mass Spectrom.* **2007,** *267,* 167–182.
57. Ruan, C.; Yang, Z.; Hallowita, N; Rodgers, M. T. Cation-π Interactions with a Model for the Side Chain of Tryptophan: Structures and Absolute Binding Energies of Alkali Metal Cation-Indole Complexes. *J. Phys. Chem. A* **2005,** *109,* 11539–11550.
58. Ruan, C.; Yang, Z.; Rodgers, M. T. Cation-π Interactions with a π-excessive Nitrogen Heterocycle: Structures and Absolute Binding Energies of Alkali Metal Cation-Pyrrole Complexes. *Int. J. Mass Spectrom.* **2007,** *267,* 233–247.
59. Laughton, C. A.; Luque, F. J.; Orozco, M. Counterion Distribution Around DNA Studied by Molecular Dynamics and Quantum Mechanical Simulations. *J. Phys. Chem.* **1995,** *99,* 11591–11599.